Soft Matter

PAPER

View Article Online
View Journal

Cite this: DOI: 10.1039/d5sm00761e

Revealing the dynamic and thermal behaviors of supercooled droplet impinging on surfaces with varying wettability

Haipeng Zhang, Jorge Ahumada Lazo, MD Sohaib Bin Sarwar and Yang Liu *

Icing caused by supercooled droplet impinging and freezing poses a serious weather hazard to aviation and many infrastructure systems, yet remains poorly understood and challenging to address. In this paper, a comprehensive experimental study was conducted to characterize the transient dynamic and thermal behaviors of supercooled droplets impinging and freezing on surfaces with varying wettability, *i.e.*, hydrophilic and hydrophobic surfaces. Both high-speed imaging and infrared thermal imaging were performed to capture the transient hydrodynamics and thermal details of supercooled droplets impinging on the different surfaces, with particular focus on the sequential stages in impinging dynamics, the unsteady heat transfer during impinging and freezing, and their competing mechanisms in determining the final ice structure formation and morphology. Our observations revealed that supercooled droplets undergo an accelerated nucleation and solidification process upon impact. Compared to regular non-cooled droplet, supercooled droplets impinging and freezing form a smaller ice roughness element on hydrophilic surfaces, while producing a much larger and rougher ice structure on hydrophobic surfaces. Additionally, it has been observed that when a supercooled droplet impacts with a reduced Weber number, it experiences a prolonged freezing period (lasting beyond the dynamic timescale of impingement), resulting in the formation of the "flying ice peanut" morphology. These findings offer new insights into the fundamental mechanisms of supercooled droplets impinging and freezing on different surfaces and provide a valuable basis for the development of more robust and effective anti-icing surface technologies.

Received 25th July 2025,
Accepted 7th October 2025

DOI: 10.1039/d5sm00761e

rsc.li/soft-matter-journal

1. Introduction

Ice accretion occurs when water droplets impinge and freeze on surfaces exposed to sub-freezing conditions. For example, in aviation, when aircraft fly through a cloud with suspended water droplets in a cold climate, the droplets impact, deposit, solidify, and accrete on aircraft surfaces, forming ice layers of various shapes that can significantly disturb the airflow.[1] As a result, the aerodynamic properties of the critical aircraft components, particularly the wings, control surfaces (ailerons, elevators, and rudders), engines, and propellers, degrade rapidly, which can lead to a sudden drop in lift and a dramatic increase in drag, and sometimes a severe early stalling of the aircraft.[2] In particular, when the diameter of a supercooled droplet exceeds 1 mm, it is classified as a supercooled large droplet (SLD), a phenomenon of critical concern in aviation. Unlike smaller cloud droplets that typically freeze upon impact near the leading edges of aircraft surfaces, SLDs have greater inertia and can travel beyond protected regions. This leads to abnormal ice accretion patterns, including runback icing, which is not adequately addressed by conventional ice protection systems. The presence of SLDs has been directly associated with severe in-flight icing events and has been shown to significantly reduce an aircraft's lift-to-drag ratio and rate of climb capability.[3,4] Beyond aviation, icing has also been recognized as a severe weather hazard for many infrastructures, including but not limited to wind turbines,[5–7] power towers and transmission cables,[8] and bridges.[9,10]

Over the past years, significant efforts have been made to address icing-related challenges, leading to the development of various anti-icing coatings and surfaces aimed at mitigating ice formation and accretion.[11,12] Among these, hydrophobic (and superhydrophobic) coatings/surfaces have gained widespread use across many applications,[13] largely due to extensive research and ongoing material innovations in the field.[14–16] These surfaces are inspired by the outstanding self-cleaning capability of the lotus leaf and duck features, which feature rough micro/nanoscale surface textures.[15] When a macroscale water droplet comes in contact with such a surface, air pockets

Department of Mechanical Engineering, The City College of New York, New York, USA. E-mail: yliu7@ccny.cuny.edu

would be formed in the surface texture beneath the droplet, leading to the high contact angles of the droplet (*i.e.*, $>100^\circ$ for hydrophobic surfaces and $>150^\circ$ for superhydrophobic surfaces). Microstructure patterns on the surface also affect the evolution of impinging droplets.[17,18] As a result, such surfaces can effectively repel droplet impingement, delay freezing, and reduce ice adhesion strength.[19–21] However, while these coatings/surfaces exhibit extraordinary anti-icing performances under static icing conditions (*i.e.*, in which ice layers are typically formed through condensation and slow freezing, or direct frost deposition from water vapor), they become ineffective under dynamic icing conditions where droplets brutally impinge and freeze on these surfaces.[22]

In real-world dynamic icing environments, such as those encountered in aviation or wind energy systems, the droplets impinging on surfaces undergo complex and transient stages, including spreading, recoiling, rebounding, splashing, and fragmentation.[23,24] The nature of these interactions is highly dependent on the impact Weber number ($We = \rho V^2 D/\gamma$, where ρ is the density of the water droplet, V is the impact velocity, and γ is the surface tension of the droplet), which quantifies the relevant significance between inertial and surface tension forces during droplet impact, as well as the surface wettability (*i.e.*, hydrophilic or hydrophobic).[25] Under freezing conditions, droplets can solidify and adhere to a surface at any point during the impinging process, depending on the ambient and surface conditions. The situation becomes significantly more severe when the droplets are supercooled. It has been found that when a cold surface encounters a cloud of supercooled droplets, such as during in-flight aircraft icing, previously effective hydrophobic anti-icing coatings can lose their functionality and degrade rapidly.[22]

Many studies have been conducted to tackle the complex physics governing the freezing of supercooled droplets. The early work by McDonald[26] examined the homogeneous nucleation of supercooled water and outlined the thermodynamic and molecular-kinetic nature of the nucleation process. Jung *et al.*[27] experimentally studied the mechanism of supercooled droplet freezing on surfaces, and established the relations between surrounding humidity and flow conditions and the freezing process of supercooled droplets. The work revealed that the environmental conditions can strongly affect the nucleation type and ice crystallization of supercooled droplets. Wang *et al.*[28] evaluated the effect of mechanical impact on the nucleation process of supercooled water. It was found that the nucleation rate of supercooled water can be enhanced upon impact, primarily due to the reduction of the free energy barrier for nucleation. Recently, Zhang *et al.*[29] studied the impinging-freezing dynamics of supercooled water droplets on cold surfaces, and developed a morphology map of rebound and adhesion of supercooled droplets on hydrophobic surfaces, correlating the Weber number, supercooling degree and contact angle. While these previous works provided great fundamental understanding of the nucleation and crystallization mechanisms of supercooled droplets and revealed the factors influencing the freezing processes of supercooled droplets, many transient details, such as the impinging hydrodynamics and the coupled thermal evolutions in the rapid phase change process, as well as their resulting outcomes, are still not well understood, particularly with regard to the comparative processes of supercooled droplets impinging and freezing on surfaces with varying wettability and their resultant ice roughness formation.

In this paper, we focused on characterizing the transient dynamic and thermal behaviors of supercooled droplets impinging on cold surfaces with varying wettability. Using a customized supercooled droplet generation system in a freezing chamber, we produced well-defined droplets with controlled supercooling degrees. The droplet diameter was larger than 1 mm, and the Weber number in the present experiments was approximately $We \approx 200$. While this range is lower than the high-We conditions typically encountered in real-world icing environments (*e.g.*, aviation or wind energy systems), it provides an essential platform for investigating the fundamental mechanisms of droplet impinging and freezing under well-controlled conditions. The insights obtained here, particularly regarding the interplay between droplet impinging dynamics and disturbance-induced rapid freezing of supercooled droplets, offer valuable reference points for extending the understanding of supercooled droplet behavior to higher We regimes. Beyond icing situations, the results also remain relevant to other low-We applications such as spray cooling, coating, and inkjet printing, where supercooled droplet interactions are of practical importance.

In this study, both high-speed imaging and infrared thermal imaging were applied to directly capture the hydrodynamic process and thermal evolution of supercooled droplets impacting surfaces with varying wettability. These results were systematically compared with those of non-cooled droplets to highlight the distinctive role of supercooling. By analyzing the transient temperature rise associated with latent heat release, we were able to quantify the freezing timescales of supercooled droplets on different substrates. Furthermore, changes in surface morphology following droplet freezing were characterized using surface roughness parameters, providing a quantitative measure of residual ice roughness formation. Together, these findings establish a mechanistic framework for understanding impingement-induced freezing of supercooled droplets.

2. Materials and methods

2.1 Materials

In this study, deionized (DI) water was used as the working fluid to generate supercooled droplets in the experimental setup. The density (ρ), viscosity (μ), and surface tension in air (γ) of DI water were taken as $\rho = 1000$ kg m^{-3}, $\mu = 1.788 \times 10^{-3}$ N s m^{-2}, and $\gamma = 75.64 \times 10^{-3}$ N m^{-1} at approximately 0 °C and 1 atm pressure.[30,31]

Aluminum plates (55 mm × 50 mm × 1 mm) with varying surface wettability were used as substrates for droplet

impingement. For preparation, the aluminum plates were first polished with sandpaper (800 and 2000 grit) and then painted with black paint (Painter's Touch Ultra Cover 2 ×, Paint + Primer, Flat Black, Rust-Oleum) to create hydrophilic surfaces. After the paint dried, an additional waterproof spray (NeverWet Multi-Purpose Spray Kit, Rust-Oleum) was applied to produce hydrophobic surfaces. The static contact angles (θ) of DI water on the hydrophilic and hydrophobic substrates were measured to be 38.50° and 131.11°, respectively, at room temperature (≈22 °C), using the $\theta/2$ method with image processing techniques.[32]

2.2 Methods

2.2.1 Experimental setup and procedures. As shown in Fig. 1, a commercial freezer with a transparent glass door (LSD-60 Household Display Freezer, Ningbo Hicon Industry Technology Co., Ltd) was used to build the experimental setup. The internal temperature of the freezer was maintained between −10 and −15 °C, as monitored using a thermometer. In practice, a ±2 °C temperature fluctuation was observed in the freezer chamber.

Prior to each experiment, the substrate was placed inside the freezer chamber to equilibrate with the environment, achieving a uniform surface temperature ($T_s \approx -8$ to -10 °C). To enhance illumination, a mirror was placed behind the substrate to reflect light from an external LED source (RS-5620, RPS Studio CooLED 200 Studio Light, Dot Line Corp.) into the chamber.

DI water droplets were generated using a long needle (20 Gauge Stainless Steel, 10 inches) inserted through the freezer door. The needle was connected *via* tubing to a syringe (10 mL Plastic Syringe, BD) filled with DI water, which was mounted on a syringe pump (NE-300 Syringe Pump, New Era Pump Systems, Inc.). As water was injected, a droplet formed at the needle tip and grew until it reached a size large enough to detach. In this study, the initial droplet diameter (D_0) was measured to be 3.13 ± 0.01 mm.

The syringe pump was operated at a low flow rate (Q = 0.1 mL min^{-1}), allowing precise control over the droplet's residence time at the needle tip and, consequently, its temperature (T). A droplet released immediately after formation had a temperature of approximately T = 0 to −4 °C, while a droplet suspended at the tip for about 5 minutes cooled to T = −8 to −10 °C. A thermocouple (DT304 Apollo IV Digital Temperature Logger, UEi Test Instruments) was used to confirm the temperature change of the suspended droplets inside the freezer. After detachment, the droplet fell onto the substrate. The impact velocity (V) was controlled by adjusting the needle height (*i.e.*, the falling distance, H_d). For instance, at H_d = 268 mm, the impact velocity was measured to be V = 2.16 ± 0.01 m s^{-1}. Thus, We = 193 in this study.

The impingement process was recorded from two perspectives: a thermal camera (FLIR A655sc, FLIR Systems AB) mounted inside the freezer captured a top view, while a high-speed camera (Phantom VEO 340L) recorded a side view through the transparent freezer door. Temperature changes over time were analyzed using the software of the thermal camera (FLIR ResearchIR), and the high-speed images were processed using MATLAB.

2.2.2 Image processing methods. When droplets impinge on the substrates, they undergo a series of deformations, including spreading, receding, and bouncing. The evolution of the droplet shape during impingement is quantified by measuring changes in droplet diameter (D) and height (H) over time (t). Custom MATLAB scripts were developed to extract these measurements from high-speed camera images.

First, a reference background image without any droplet was captured from the experimental setup and saved as I_0. After importing I_0 and the high-speed camera images into MATLAB, each frame of high-speed camera images containing a droplet (*e.g.*, I_1) was processed by computing the absolute pixel intensity difference: $I = \mathrm{abs}(I_0 - I_1)$.

This operation removes the background, isolating the droplet in the resulting image I. The processed image is then converted

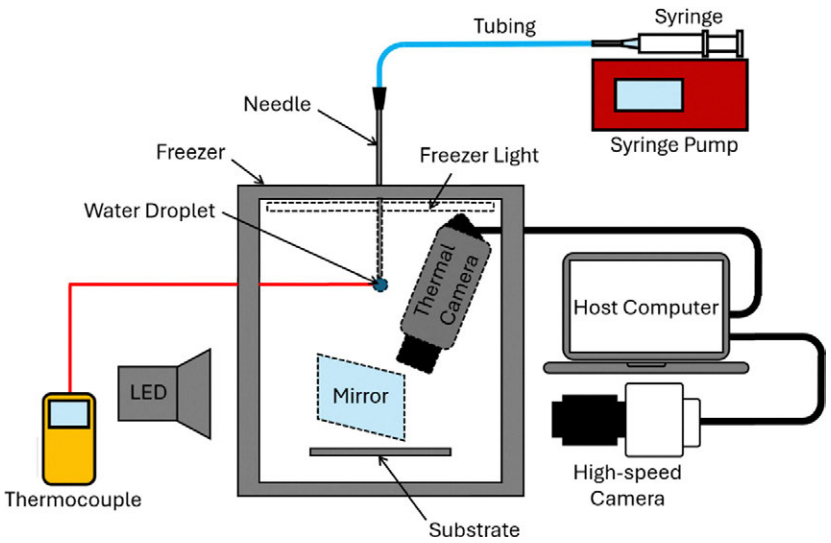

Fig. 1 Schematic diagram of experimental setup.

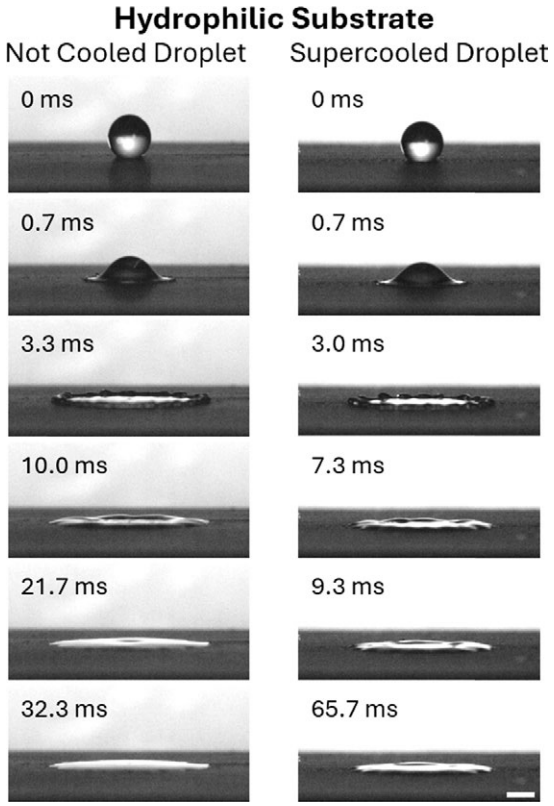

Fig. 2 Time sequence images of droplet impingement on hydrophilic substrates (scale bar: 2 mm). The impact velocity of droplets was measured as $V \approx 2.16$ m s^{-1}, We $\approx$ 200. (left) Droplet was not cooled ($T \approx 4$ °C); (right) supercooled droplet ($T \approx -8$ °C).

into a binary format using 'imbinarize' function. The droplet boundary in each frame is identified using 'bwtraceboundary' function, allowing the boundary of the droplet to be tracked over time.

Based on the detected boundaries, the initial droplet diameter before impingement (D_0) and the dimensions (D and H) of the droplet during and after impingement were measured. D_0 was determined by applying a Kasa method-based circular fitting algorithm to detected droplets, yielding an averaged droplet diameter.[33,34] D was defined as the horizontal distance between the leftmost and rightmost points of the droplet boundary, while H was measured as the vertical distance from the droplet's top edge to the substrate surface. In cases where the droplet bounced off a hydrophobic surface, H could exceed the droplet's actual height, indicating that the droplet had detached from the substrate.

3. Results and discussion

3.1 Transient hydrodynamics of supercooled droplets impinging on hydrophilic and hydrophobic surfaces

As mentioned previously, when a droplet impinges on a substrate, it typically experiences spreading and receding (or rebounding) processes. When the surface temperature of the substrate is sub-freezing, this deformation process occurs simultaneously with the freezing of the droplet. Fig. 2 illustrates the impingement and corresponding deformation process of two different droplets (*i.e.*, not-cooled droplets *vs.* supercooled droplets) impinging on hydrophilic surfaces. The impact velocity of the droplets on the substrate was $V \approx 2.16$ m s^{-1}. Under this condition, the Weber number of the droplet impingement was calculated to be We $\approx$ 200. At room temperature, droplet impingement with such a We value is referred to as a deposition pattern. In this mode, the droplet spreads along the surface of the substrate after initial contact, reaches its maximum spreading diameter, and then recedes back to a static state, forming a spherical cap-like shape. During this process, no bouncing or splashing of the droplet occurs.[23,35,36]

In Fig. 2, the left column shows a droplet without supercooling, while the right column shows a supercooled droplet. For the non-cooled droplet, it is clear that spreading occurs immediately after initial contact with the substrate. A lamella rim with a wavy boundary forms and grows rapidly as the droplet is at room temperature.[35] From the captured images, the droplet reaches its maximum spreading diameter at t = 3.3 ms, and this maximum diameter can be predicted using only impingement parameters, such as the Reynolds number (Re) or We.[23,37]

Afterward, the droplet recoils, and capillary waves form and propagate along its surface. These waves can deform the droplet into a pyramidal structure. Then, the droplet undergoes oscillations, alternating between a flattened disk-like shape and a semi-spherical cap shape. These fluctuations gradually decay due to dissipative mechanisms, such as viscous damping, until the droplet reaches a steady state. The oscillation process and the final equilibrium configuration depend on parameters including droplet viscosity, impact velocity, and substrate wettability.[38–40]

Meanwhile, the initial freezing process takes place. As previously observed, a thin layer of ice forms at the bottom of the spreading droplet, pinning its spreading boundary. Thus, when the liquid phase begins to recede toward the center of the droplet, the outer boundary shows negligible change. However, this does not mean that the entire droplet freezes immediately. The freezing process starts from the bottom and progresses layer by layer.[41] As shown at t = 21.7 ms, oscillations continue in the unfrozen liquid phase above the frozen layer. The freezing process completes after the droplet reaches a steady status, with a smooth surface profile.

When the droplet is supercooled, the initial impact and spreading behavior on the substrate are very similar to the non-cooled case. The most significant difference is observed after the droplet reaches its maximum spreading diameter. As shown in the right column of Fig. 2, the wavy-shaped lamella rim ceases its oscillatory motion and maintains the same pattern from t = 9.3 ms onward. This suggests that the freezing process occurs on a much shorter timescale, approximately 10 ms, before the oscillatory motion of the unfrozen liquid phase can create a smooth surface on the top of the droplet.

This rapid freezing of the entire droplet is considered to be a characteristic response of supercooled droplets. When the

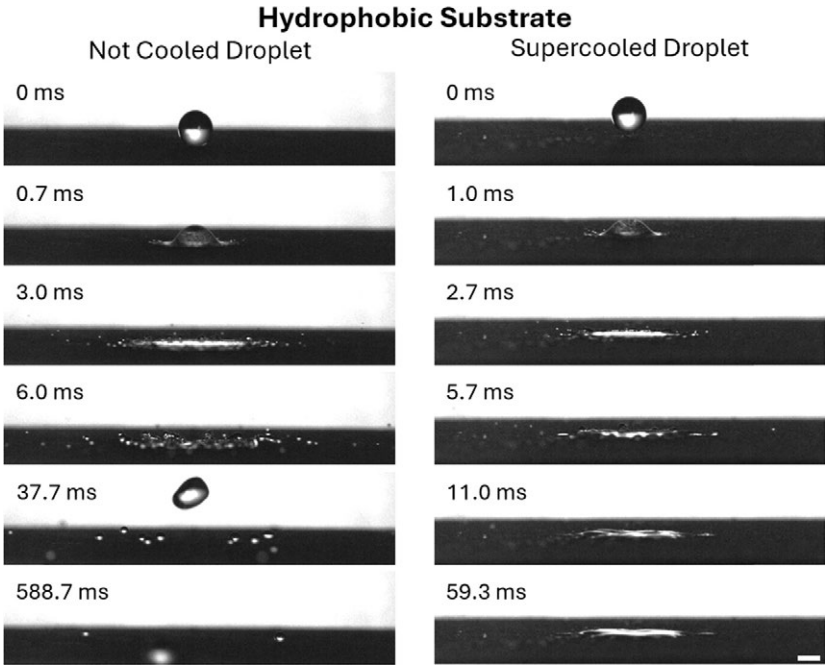

Fig. 3 Time sequence images of droplet impingement on hydrophobic substrates (scale bar: 2 mm). The impact velocity of droplets was measured to be $V \approx 2.16$ m s^{-1}, We ≈ 200. (left) Droplet was not cooled ($T \approx 4$ °C); (right) supercooled droplet ($T \approx -8$ °C).

droplet is below the freezing point prior to impingement, it exists as a mixture of liquid and ice crystals. This is an unstable state, which can be triggered by any disturbance. In this case, the impingement acts as the disturbance that initiates the freezing process.[27,29]

Fig. 3 illustrates the results of another experiment involving droplet impingement on hydrophobic substrates. The left column shows the impingement and evolution process of a droplet without cooling on the substrate. It is clear that even though the droplet impingement occurred in a sub-freezing condition, no visible freezing process was observed during the recorded time period. After initial contact, the droplet spread on the substrate and reached its maximum spreading diameter at $t = 3.0$ ms, which was the same timescale as shown in Fig. 2. This supports the statement that the spreading behavior of a droplet can be predicted solely based on the impact conditions and is less influenced by surface properties of substrates.[37]

Afterward, the droplet ruptured into multiple small droplets as it began to recede toward the center of impact. In the meantime, these droplets bounced off the substrate. Some of the ruptured droplets coalesced and formed a larger droplet at the center. This droplet bounced on the substrate multiple times before leaving the field of view of the high-speed camera. Afterward, the droplet could undergo a heat transfer process and eventually freeze when it comes to rest at some location on the substrate.

A significantly different phenomenon was observed in the case of supercooled droplets, as shown in the right column of Fig. 3. A similar initial contact and spreading process to that of the non-cooled droplets was observed at the early stage of impingement. However, the droplet did not undergo any receding, rupturing, or lift-off behavior. Instead, after t = 5.7 ms, the droplet appeared to retain its spreading pattern on the substrate and stopped further motion. The droplet was found to freeze immediately after reaching its maximum spreading diameter on the substrate.

Fig. 4 summarizes the image processing results of two parameter to quantify the evolution of droplets after impingement, the diameter (D) and the height (H) of the droplet over time (t). Here, D indicates the maximum value of the droplet's diameter, and H indicates the maximum height of the droplet from the substrate. When the droplet bounces off the substrate, D differs from the diameter of the droplet in contact with the surface, and H can be larger than the vertical dimension of the droplet itself.

As shown in Fig. 4(a), on both hydrophilic and hydrophobic substrates, the droplet diameter increased rapidly after initial contact. For all cases, the duration of this rapid increase was similar. Afterward, the D of a droplet without cooling gradually decreased over time on the hydrophilic substrate. This corresponds to the receding process of the droplet on the surface. However, when the droplet was supercooled, D became constant after the initial spreading on the substrate. A similar trend was also observed for the supercooled droplet on the hydrophobic surface. This indicates that the droplet began freezing on the substrate shortly after impingement, effectively arresting its spreading and causing the measured diameter, D, to remain essentially constant thereafter. The fingering patterns formed along the droplet perimeter on the hydrophobic surface (as can be seen in the top-view images of droplet impingement in Fig. 5), combined with partial freezing during spreading, contributed to the slightly larger diameter compared to hydrophilic

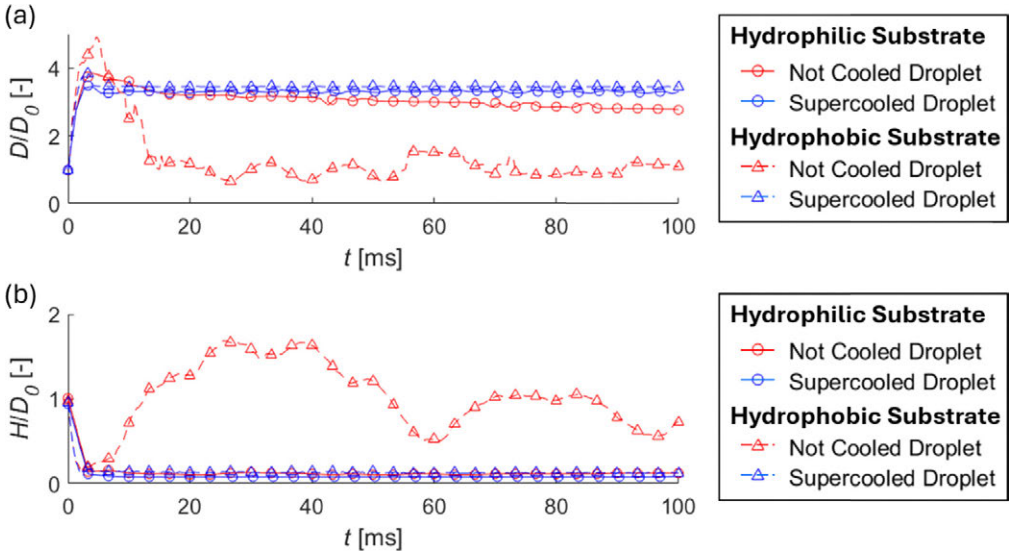

Fig. 4 The evolution of droplets on different substrates after impingement. (a) Normalized diameter change of the droplet (D/D_0) over time (t); (b) normalized height change of the droplet (H/D_0) over time (t).

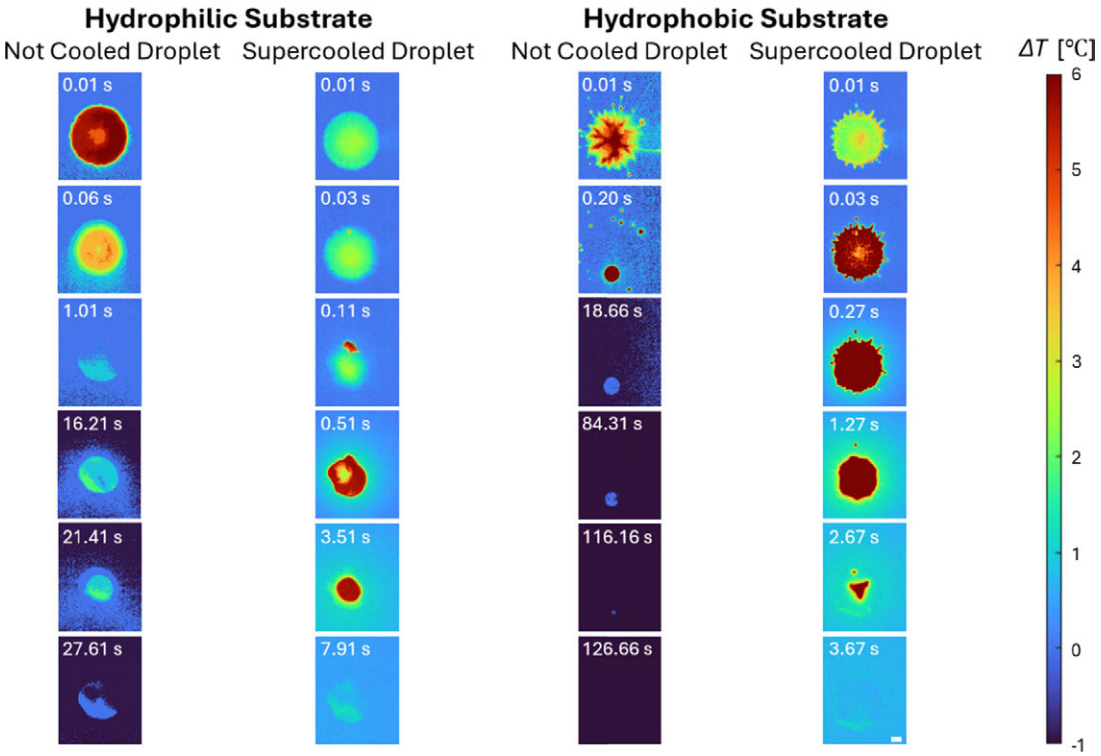

Fig. 5 Time sequence images of relative temperature evolution of impinged droplets (ΔT) on substrates (scale bar: 2 mm). The impact velocity of droplets was measured as $V \approx 2.43$ m s^{-1}, We ≈ 245. (left) Droplets on hydrophilic substrates; (right) droplets on hydrophobic substrates.

surfaces. In contrast, for the non-cooled droplet impinging on the hydrophobic substrate, D exhibited significant periodic fluctuations due to the bouncing and oscillatory motion of the droplet.

The height of the droplet provides similar information. As shown in Fig. 4(b), for supercooled droplets—whether on hydrophilic or hydrophobic substrates—H rapidly decreased and quickly reached a constant value immediately after impingement. The trends and values of H were very similar to those observed for a droplet without cooling on the hydrophilic substrate. This behavior is completely different from that of a non-cooled droplet on a hydrophobic substrate, where the droplet continuously bounced on the surface periodically.

3.2 Thermal evolutions of supercooled droplets impinging and freezing on hydrophilic and hydrophobic surfaces

From experimental observations, we found that supercooled droplets stopped changing shape within a short time after impingement. This observation was further confirmed by the quantitative analysis of D and H. It is believed that the cessation of droplet deformation was due to the rapid freezing of the supercooled droplet, triggered by the disturbance during the impingement process. To verify this hypothesis, the thermal evolutions of droplets were measured using a thermal camera, as described below.

Fig. 5 summarizes the temperature variations of droplets on various substrates over time (t). To highlight the thermal evolutions of the impinging and freezing droplets as indicated by the temperature changes, the relative temperature of the droplets (ΔT) was used, which was calculated based on the difference between the measured droplet temperature and the initial substrate temperature immediately before droplet impact. In this study, the substrate temperature was maintained at $T_s \approx -8$ to -10 °C.

From Fig. 5 (left), it was observed that for a non-cooled droplet, the outer boundary receded after impingement. The droplet formed a sessile shape on the substrate, and its overall temperature gradually decreased. The relative temperature (ΔT) of the droplet reached zero after approximately 1 s. Subsequently, the formation of a freezing layer at the bottom of the sessile droplet was observed at around t = 16.21 s. A slight increase in temperature during this process suggested that latent heat was released from the freezing layer within the droplet; however, this increase was not significant compared to other cases. Eventually, as the freezing process progressed, the temperature of the droplet approached that of the substrate again.

However, for a supercooled droplet, in addition to the outer boundary being pinned after spreading, a temperature increase was detected from t = 0.11 s, indicating the onset of the nucleation process. It was clear that the entire droplet had completed nucleation by around t = 0.51 s.[27,42] After freezing, the temperature of the droplet gradually decreased again, due to heat transfer between the droplet and the surroundings, known as the cooling process. From these images, it is evident that nucleation of the supercooled droplet occurred at t = 0.11 s, which is much faster than that observed in non-cooled droplets.

Similar observations were made from Fig. 5 (right). For a non-cooled droplet, after impinging on the hydrophobic surface, it ruptured into multiple small droplets that scattered across the surface. The temperature of each droplet decreased over a longer time through the heat transfer process.[43] It was seen that, a spherical droplet resting on the hydrophobic surface required more than 120 s to reach thermal equilibrium with the substrate. This is primarily due to the smaller contact area (with a large contact angle) and the taller droplet beading up on the hydrophobic surface, which substantially increases the thermal resistance in heat conduction to remove the latent heat of fusion during the freezing process. Over this prolonged freezing period, the substrate surface experienced a slight variation in temperature as indicated by the temperature maps.

For the supercooled droplet, however, a low-temperature region at the outer boundary upon droplet impact indicated that the spreading edge had been pinned to the substrate. In addition, a clear temperature increase in the central region of the droplet was observed at t = 0.03 s, again indicating the occurrence of the nucleation process. Compared to the non-cooled droplet case, the freezing of supercooled droplets occurred over a much shorter timescale following impingement. Moreover, no droplet breakup and fragmentation were seen in the case of supercooled droplet impinging on the hydrophobic surface. The significantly accelerated nucleation and freezing effectively locked the impinging droplet on the surface.

From the captured thermal images, the average relative temperature of droplets (ΔT) was obtained from the spreading region on the substrates in each thermal frame. Here, the initial surface temperature of the substrate (T_s) was used as the reference temperature. In our experiments, T_s was typically -8 to -10 °C and remained relatively stable during the short duration of each test, with only minor variations (≈ 2 °C) observed over longer periods due to the operational limits of the freezing chamber. Because the impingement and freezing of supercooled droplets occur on a sub-second timescale, these small fluctuations have negligible influence on the transient dynamics and rapid solidification of supercooled droplet cases reported here. However, for non-cooled droplets, the freezing process occurs over a much longer timescale, and substrate temperature variations may therefore become more noticeable during the process. When the chamber temperature dropped below the initial substrate temperature (T_s), ΔT would become negative, as seen in the non-cooled droplet cases in Fig. 6. The results were plotted over time (t), as shown in Fig. 6. From the plot, for a non-cooled droplet on a hydrophilic substrate, it was clearly seen that ΔT decreased immediately after impingement, representing the initial cooling process. At t = 15 s, a sudden increase in ΔT was observed. This temperature rise was caused by latent heat of fusion released during the freezing of the droplet, providing a reference timescale indicating that the freezing process required more than 10 seconds after impingement for non-cooled droplets. As shown in the inset of Fig. 6, a similar ΔT increase can also be observed in supercooled droplets during the early stage after impingement on hydrophilic and hydrophobic substrates, respectively. After that, ΔT gradually decreased again, corresponding to the cooling of the frozen droplet.

It is noteworthy that identifying the increase in ΔT and the duration of latent heat release for the non-cooled droplet impacting the hydrophobic substrate is challenging based on the data presented in Fig. 6. This is because the freezing process of a non-cooled droplet was accompanied by dynamic behaviors such as droplet breakup and bouncing, which introduced complexity into the analysis.

For supercooled droplets, a rapid and distinct increase in ΔT was consistently observed at the very early stage of the thermal

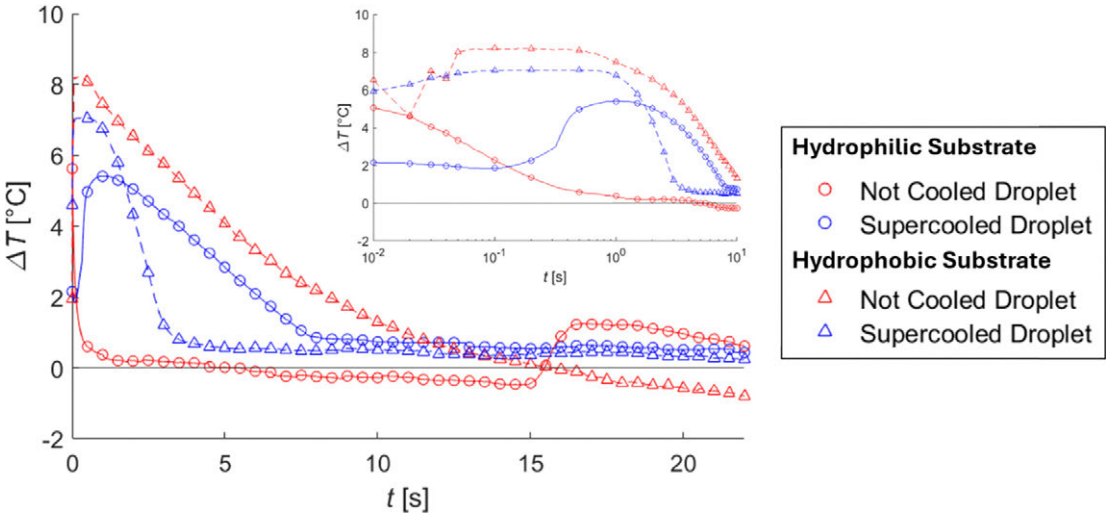

Fig. 6 The relative temperature evolution of droplets (ΔT) on different substrates after impingement over time (t) (inset: A linear-log plot of ΔT from t = 0.01 to 10 s).

profile, immediately following impingement on the surfaces. This sudden temperature increase indicates the onset of ice nucleation, which is a highly exothermic process due to the latent heat of fusion released during phase change. It should be noted that the sharp rise in ΔT was evident regardless of the surface wettability, on both hydrophilic and hydrophobic surfaces. This suggests that the initial nucleation mechanism is primarily governed by the thermodynamic state of the droplet rather than surface properties. Experimental observations indicate that nucleation typically occurred within 10 to 100 milliseconds after impact. This rapid initiation highlights the metastable nature of supercooled droplets, where even minor disturbances, such as contact with a solid surface, can trigger instantaneous phase transition. Following nucleation, the solidification process was generally completed within several seconds.

In contrast, there was no clear indicator in the obtained ΔT profile to determine the nucleation time for non-cooled droplets on hydrophobic substrates. This was due to the oscillatory motion of the droplet on the substrate. Although the temperature of the droplet showed a decreasing trend, the freezing process required a much longer time than recording, occurring only after the droplet had ceased bouncing and remained stationary.

In summary, two competing mechanisms were identified in the freezing process of an impinging droplet: the fluid dynamic process and the disturbance-induced freezing process, each governed by distinct time scales. The fluid dynamic process is primarily controlled by impact conditions such as the Weber number, while the freezing process is governed by the thermal state of the droplet (*e.g.*, whether it is supercooled and the degree of supercooling) together with the heat transfer characteristics at the droplet/substrate interface.

For a non-supercooled droplet, the solidification timescale is much longer than the droplet's impingement dynamics, so freezing occurs only after spreading, receding, or rebounding are completed on the substrate. In contrast, for a supercooled droplet, the solidification timescale is significantly reduced, allowing freezing to initiate during the dynamic phase of impact. This rapid freezing alters the impingement outcome, producing effects such as suppressed bouncing or incomplete breakup on hydrophobic substrates.

It is worth mentioning that the degree of supercooling also plays a critical role in determining both the onset and progression of the freezing process during droplet impingement. At lower supercooling degrees, the nucleation barrier is relatively high, so freezing may be initiated only after a noticeable delay. In such cases, the droplet may spread, retract, or even partially bounce before solidification occurs, resulting in weaker ice adhesion and reduced frozen mass on the substrate. At higher supercooling degrees, however, the nucleation barrier is significantly lowered, leading to almost instantaneous freezing upon impact. This rapid solidification can interfere with the normal impingement dynamics by arresting spreading, suppressing retraction, and preventing rebound, even on hydrophobic surfaces. The outcome is a larger amount of liquid being captured and frozen onto the substrate, which enhances the potential for ice accumulation. A critical regime may exist where the two time scales, fluid dynamics and freezing, are comparable, dictating whether the droplet freezes on the substrate or solidifies after rebounding in flight. This work highlights the importance of supercooling in dictating freezing outcomes, and future studies will further investigate the effects of supercooling degrees on these transitions to provide a more quantitative understanding.

3.3 Effects of rapid freezing of supercooled droplets on the ice roughness morphologies

From the thermal images, it was confirmed that the nucleation and freezing process of supercooled droplets was triggered by the disturbance during droplet impingement, and that the freezing occurred more rapidly than in non-cooled droplets. Due to this short freezing timescale, the spreading and subsequent

oscillatory motion of the droplet after impingement were also affected by the freezing process. As a result, the droplet may not reach a steady state with a smooth, spherical cap-like shape. Instead, freezing occurred during the fluidic motion of the lamella rims, which can lead to irregular deposition patterns on the substrate and significantly increase surface roughness.

Fig. 7 and 8 show the side-view profiles of hydrophilic and hydrophobic substrates with non-cooled and supercooled droplets frozen on them, respectively. The blue solid lines indicate smoothed surface profile curves derived using MATLAB's smooth function, which applies the Savitzky–Golay filter ('sgolay' method). Surface roughness was quantified using the parameters R_p, R_v, and R_a. For the selected area containing the spreading droplet, the height of each pixel along the droplet profile was measured, and the average height was indicated by a red solid line at the bottom of Fig. 7 and 8. R_p and R_v represent the maximum and minimum height deviations from this mean line, corresponding to a peak and a valley, respectively, as indicated by red dashed lines. R_a is the average surface roughness, which is represented by red dotted lines, calculated as the mean of the absolute differences between each surface point and the mean line.[44,45] An R_a of 0 indicates a perfectly smooth surface, while a higher R_a value corresponds to greater surface roughness.

A comparison of the side-view surface profiles of frozen droplets with different initial temperature conditions on hydrophilic substrates is shown in Fig. 7. A non-cooled droplet formed a cap-like shape after freezing on the substrate, with a smaller wetting area, whereas a frozen supercooled droplet spread more on the substrate, forming a thin disc-like shape. These are represented in Fig. 7(a) and (b), respectively. As supported by the observations in Fig. 2 and 5, the freezing process of an impinging non-cooled droplet required a longer time than that of a supercooled droplet. This allowed the droplet to undergo the complete spreading and retraction process after impingement. Consequently, freezing occurred after the droplet retracted from its maximum spreading diameter, resulting in a more bulged frozen shape on the hydrophilic substrate.

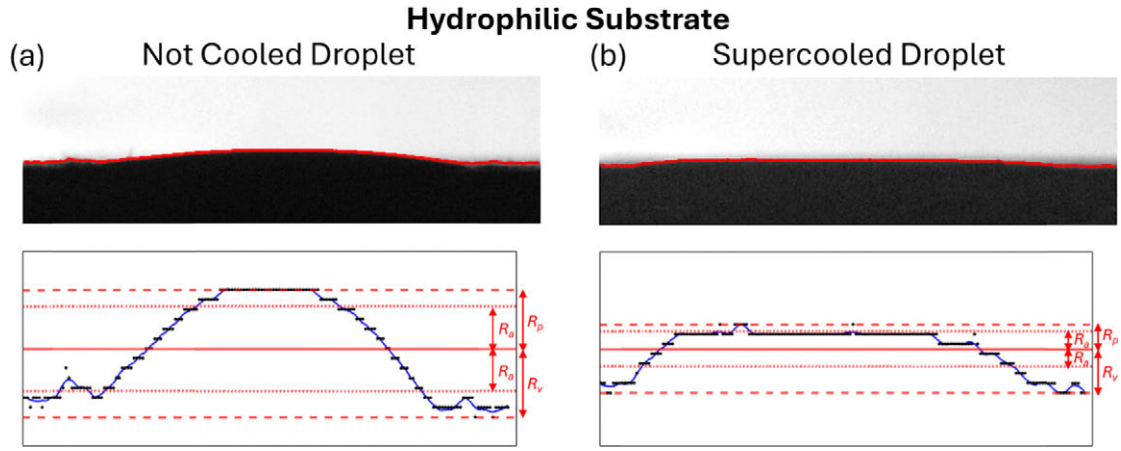

Fig. 7 The side-view profile of frozen droplets on hydrophilic substrates. (a) Non-cooled droplet; (b) supercooled droplet. The parameters of surface roughness of substrates, R_a, R_p, and R_v, are shown in Table 1.

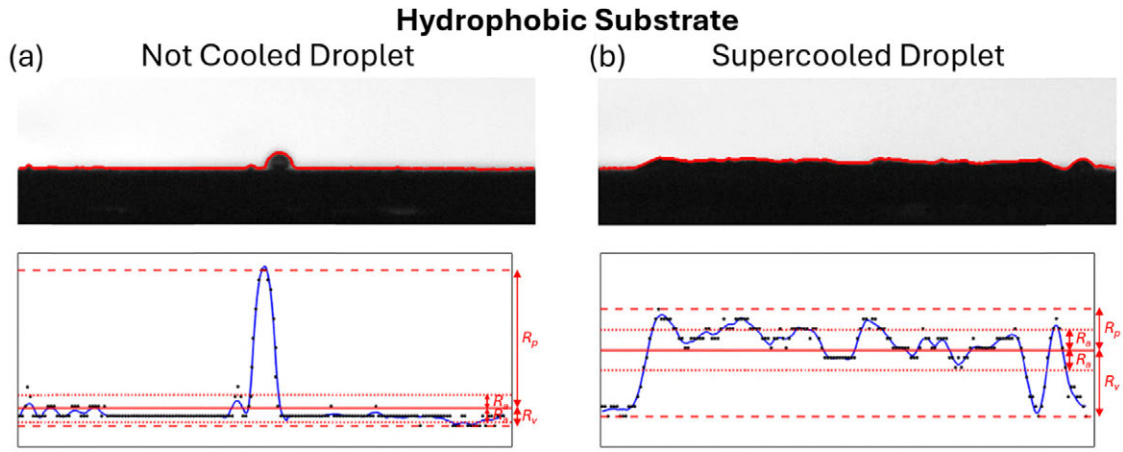

Fig. 8 The side-view profile of frozen droplets on hydrophobic substrates. (a) Non-cooled droplet; (b) supercooled droplet. The parameters of surface roughness of substrates, R_a, R_p, and R_v, are shown in Table 1.

Similarly, the side-view surface profiles of frozen droplets with different initial temperature conditions on hydrophobic substrates are shown in Fig. 8(a) and (b). For a non-cooled droplet, the freezing time scale was much longer than the transient dynamics of impingement, spreading, and breakup on the hydrophobic substrate. Before freezing occurred, the droplet fragmented into multiple smaller droplets upon impingement, many of which bounced off and exited the measurement region. Consequently, only a small fraction of the liquid remained and eventually froze into bead-like residues on the substrate. As shown in Fig. 8(a), the resulting frozen mass was significantly smaller than that observed for the supercooled droplet case. This behavior highlights the effectiveness of hydrophobic surface treatments in minimizing water retention and explains their practical use in anti-icing applications.

In contrast, the freezing process for a supercooled droplet occurred almost immediately after impingement, even on a hydrophobic substrate. The droplet solidified during the spreading stage, forming a disk-like frozen morphology as shown in Fig. 8(b). In this case, the frozen layer covered the hydrophobic coating and effectively altered the substrate's surface properties. This observation demonstrates that while hydrophobic surfaces are effective in shedding non-cooled droplets, their anti-icing efficiency is significantly compromised under supercooled droplet impingement conditions.

It is also observed that, the frozen droplet exhibited a slightly bumpy surface compared to the supercooled droplet freezing on hydrophilic substrates. This arises because the droplet solidifies while still undergoing shape fluctuations during the spreading and receding stages, which are driven by the interplay of inertial, surface tension, and viscous forces. On hydrophobic substrates, these fluctuations are more pronounced due to the high contact angle, which reduces the resistance to droplet motion and allows larger oscillations after impingement.

As a result, the droplet does not achieve a perfectly smooth shape before freezing, and the solidification effectively "locks in" the transient surface undulations, producing a slightly bumpy morphology. This behavior contrasts with that of supercooled droplets on hydrophilic substrates, where stronger wetting and higher surface adhesion suppress oscillations, leading to smoother frozen surfaces. These observations are consistent with the behaviors shown in Fig. 3 and 5 and help explain why hydrophobic coatings, while effective in shedding non-cooled droplets, may produce irregular ice morphology under supercooled droplet impingement.

The surface roughness parameters of each case after freezing of non-cooled and supercooled droplets are summarized in Table 1. For frozen droplets on hydrophilic substrates, the values of R_a, R_p, and R_v for a non-cooled droplet were higher than those for a supercooled droplet. This supports the observation that the cap-shaped frozen droplet formed from a non-cooled droplet significantly increased the surface roughness of the substrate compared to the supercooled case. In contrast, when droplet impinges and freezes on hydrophobic substrates, although a non-cooled droplet exhibited a large R_p value, both

Table 1 The measurement of surface roughness of substrates

	Hydrophilic substrate		Hydrophobic substrate	
Parameters [mm]	Not cooled	Supercooled droplet	Not cooled	Supercooled droplet
R_a	0.117	0.050	0.039	0.057
R_p	0.164	0.068	0.388	0.115
R_v	0.191	0.123	0.048	0.185

R_a and R_v were lower than those of the supercooled droplet. The high R_p was primarily caused by sudden local height changes, but only in a limited area on the substrate surface. Compared to the supercooled droplet cases, it suggests that the non-cooled droplet had negligible effects on the surface conditions after breaking up and bouncing off the substrate.

Also, it was clearly observed that the R_a induced by a frozen supercooled droplet was higher on the hydrophobic surface than on the hydrophilic surface. In other words, supercooled droplets can rapidly freeze upon impinging on hydrophobic substrates, and the resulting ice formations can substantially

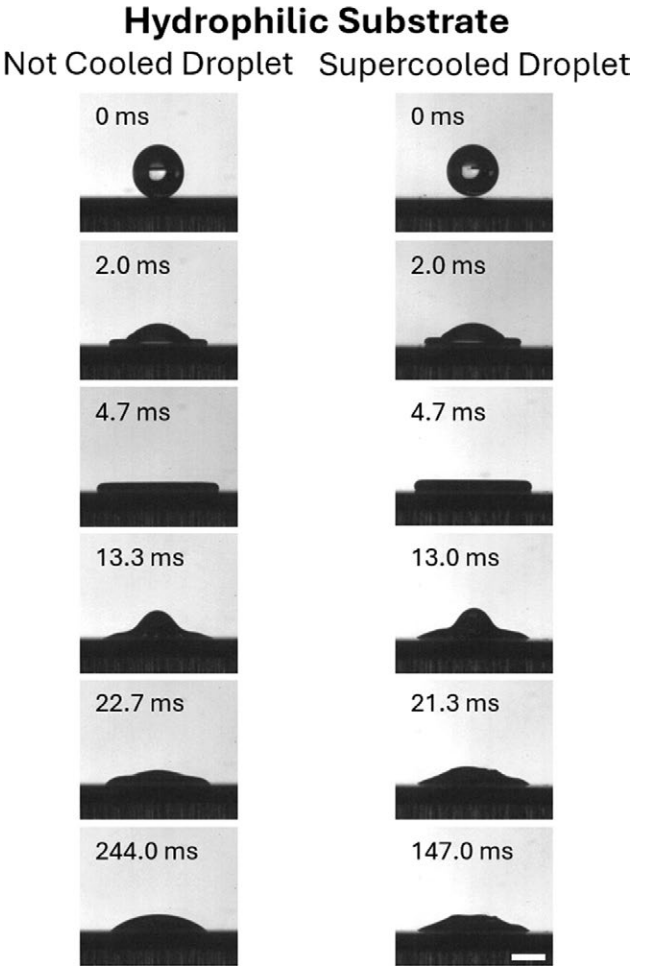

Fig. 9 Time sequence images of droplet impingement on hydrophilic substrates (scale bar: 2 mm). The impact velocity of droplets was measured as $V \approx 0.92$ m s^{-1}, We $\approx$ 35. (left) Droplet was not cooled ($T \approx 4$ °C); (right) Supercooled droplet ($T \approx -8$ °C).

increase surface roughness. This observation raises a critical concern: Are hydrophobic surface treatments truly effective for anti-icing applications, particularly when the impacting droplets are already in a supercooled state? The increased surface roughness resulting from the rapid freezing of supercooled droplet on hydrophobic surfaces could enhance the local heat convection and promote the further freezing of subsequent droplet impingement, accelerating the ice accretion on aerodynamic surfaces.[46]

3.4 Effects of impinging Weber number on the freezing of supercooled droplets

It has been experimentally demonstrated that a rapid freezing process can be initiated by the impingement of supercooled droplets on substrates. When the timescale of freezing is shorter than that of the hydrodynamics (including spreading, receding, and bouncing) of droplet upon impingement, irregular ice morphologies can form, even on hydrophobic substrates. It should be noted that all of the results presented in the previous sections are obtained at We $\approx$ 200. In this study, we also investigated droplet impingement at different Weber numbers (*i.e.*, ranging from We $\approx$ 35 to We $\approx$ 200). In the low Weber number regime, reduced disturbance during impingement was observed. The results are presented in Fig. 9 and 10.

On hydrophilic substrates, the evolution of droplet shape was similar between non-cooled and supercooled droplets until the onset of freezing in the supercooled case. Although it was difficult to pinpoint the exact moment of freezing, it was observed that freezing began at t = 21.3 ms, as shown in Fig. 9. Compared to earlier results in Fig. 2, this indicates a delayed freezing onset under lower We number conditions.

Comparable trends were observed on hydrophobic substrates. The droplet bounced off after impingement, similar to the non-cooled case. Interestingly, the nucleation process became visible at the center of the droplet as it lifted off at t = 15.3 ms, as shown in Fig. 10, suggesting that impingement still triggered freezing. However, freezing was only completed by t = 51.3 ms, after the droplet had fully detached from the substrate, leading to the formation of a ''flying ice peanut'', as clearly shown in Fig. 10. This detached-freezing phenomenon is

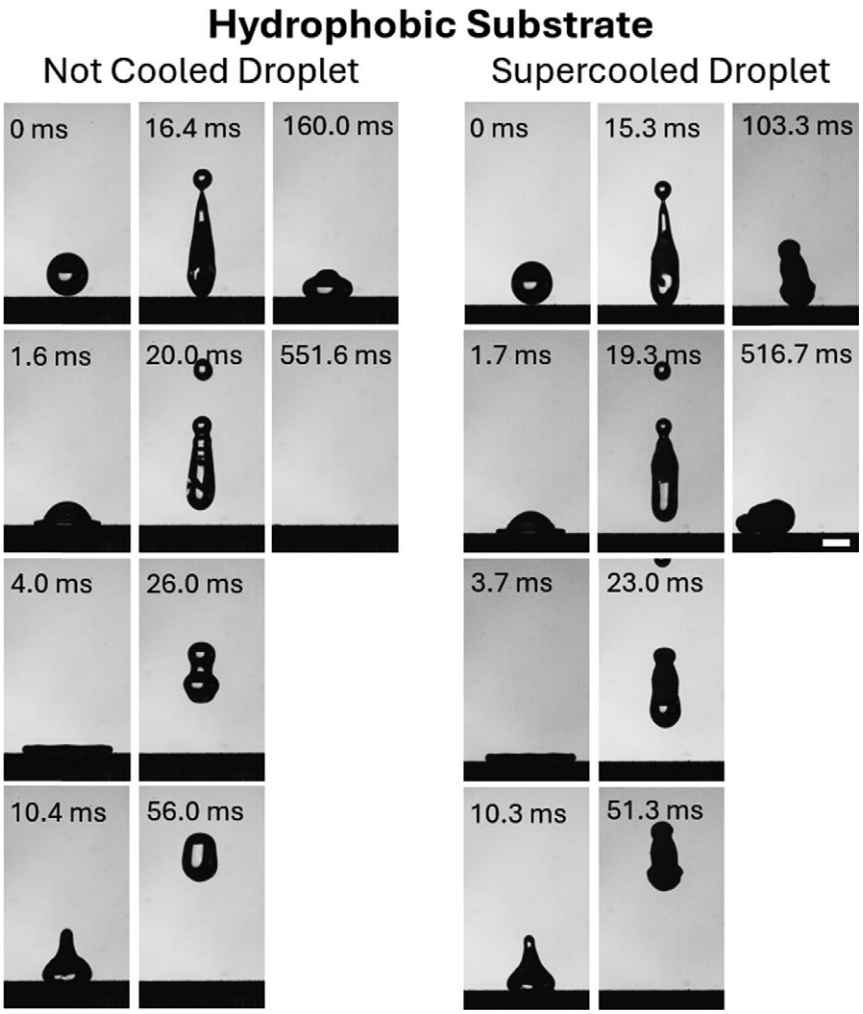

Fig. 10 Time sequence images of droplet impingement on hydrophobic substrates (scale bar: 2 mm). The impact velocity of droplets was measured as $V \approx 0.92$ m s^{-1}, We $\approx$ 35. (left) Droplet was not cooled ($T \approx 4$ °C); (right) supercooled droplet ($T \approx -8$ °C).

rarely documented in the literature and represents a unique observation of how impact dynamics and delayed nucleation can combine to suppress direct ice adhesion.

These results demonstrate that the freezing timescale of a supercooled droplet initiated by impingement is strongly dependent on the Weber number. At lower We, the freezing onset is delayed, extending the overall solidification timescale. When this timescale exceeds that of the droplet impinging dynamic processes (spreading, retraction, and rebound), solidification can occur only after detachment from the hydrophobic surface. This mechanism reduces the likelihood of ice adhesion and limits the formation of undesired surface roughness. Taken together, these findings not only confirm trends suggested in prior studies but also reveal a new pathway, detached freezing of supercooled droplets on hydrophobic surfaces, that could inform the design of advanced anti-icing strategies.

4. Conclusions

In this paper, we investigated the transient dynamic and thermal behaviors of supercooled droplets impinging and freezing on surfaces with varying wettability (hydrophilic *vs.* hydrophobic), in comparison to the impinging and freezing processes of a non-cooled droplet under the same ambient and surface conditions. We applied high-speed imaging and infrared thermal imaging to capture the transient hydrodynamics and thermal details of supercooled droplets impinging on the different surfaces. Particular attention was given to the sequential stages of droplet impact, the unsteady thermal transport, and the interplay between these processes that ultimately governs the formation and morphology of the resulting ice structures.

Under experimental conditions where droplets were impinged in deposition mode (We $\approx$ 200), rapid freezing of supercooled droplets was triggered by impingement on substrates. The droplets formed well-defined ice caps on the substrate, regardless of the surface wettability. A comparative analysis of ice roughness parameters (R_a, R_p, and R_v) reveals significant differences in the final ice roughness formation and morphology between the supercooled droplet and non-cooled droplet. On hydrophilic surfaces, the slow freezing of a non-cooled droplet produces a larger roughness element in comparison to the rapid freezing of a supercooled droplet (*i.e.*, solidifies before the droplet receding stage). In contrast, on hydrophobic surfaces, non-cooled droplets tend to break up and rebound upon impact, producing only sparsely distributed small ice fragments. These fragments are often negligible, especially under airflow conditions, as they may be easily detached from the surface. However, supercooled droplets impinging on hydrophobic surfaces freeze rapidly upon contact, resulting in substantially larger ice roughness. This significantly increased surface roughness can enhance the local heat convection and promote accelerated ice accumulation.

In addition, we also examined the effects of impinging Weber number on the freezing behavior of supercooled droplet. The results indicate a correlation between We and the freezing timescale of supercooled droplets. At a lower We number, the timescale of supercooled droplet freezing tends to be longer. For example, at We $\approx$ 35, a supercooled droplet impinging on a hydrophobic surface exhibits a freezing timescale longer than that at We $\approx$ 200, exceeding the characteristic timescale of the impinging dynamic process. That is, the droplet solidifies after it bounces off the substrate, leading to the formation of a ''flying ice peanut'', away from the surface.

These findings offer new insights into the fundamental mechanisms of supercooled droplet impinging and freezing and provide a valuable basis for the development of more robust and effective anti-icing surface technologies.

Author contributions

Haipeng Zhang: methodology, software, validation, formal analysis, investigation, writing – original draft, writing – review & editing, visualization. Jorge Ahumada Lazo: software, formal analysis. MD Sohaib Bin Sarwar: software, visualization. Yang Liu: conceptualization, methodology, resources, writing – original draft, writing – review & editing, visualization, supervision, project administration, funding acquisition.

Conflicts of interest

The authors declare no conflict of interest.

Data availability

The datasets supporting the findings of this study are available from the corresponding author upon reasonable request.

Acknowledgements

This work was supported by the U.S. Department of Energy, Office of Science, Office of Fusion Energy Sciences under Award Number DE-SC0024663, and the National Science Foundation (NSF) under Award Number 2242311.

References

1 M. B. Bragg, G. M. Gregorek and J. D. Lee, Airfoil aerodynamics in icing conditions, *J. Aircr.*, 1986, **23**(1), 76–81, DOI: 10.2514/3.45269.
2 S. K. Thomas, R. P. Cassoni and C. D. MacArthur, Aircraft anti-icing and de-icing techniques and modeling, *J. Aircr.*, 1996, **33**(5), 841–854, DOI: 10.2514/3.47027.
3 M. K. Politovich, Aircraft icing caused by large supercooled droplets, *J. Appl. Meteorol. Climatol.*, 1989, **28**(9), 856–868, DOI: 10.1175/1520-0450(1989)028<0856:AICBLS>2.0.CO;2.
4 C. Zhang and H. Liu, Effect of drop size on the impact thermodynamics for supercooled large droplet in aircraft icing, *Phys. Fluids*, 2016, **28**(6), 062107, DOI: 10.1063/1.4953411.

5 G. Fortin and J. Perron, Wind turbine icing and de-icing. 47th AIAA Aerospace Sciences Meeting including The New Horizons Forum and Aerospace Exposition, 2009, p. 274, DOI: 10.2514/6.2009-274.
6 O. Parent and A. Ilinca, Anti-icing and de-icing techniques for wind turbines: Critical review, *Cold Reg. Sci. Technol.*, 2011, **65**(1), 88–96, DOI: 10.1016/j.coldregions.2010.01.005.
7 Z. Zhang, H. Zhang, X. Zhang, Q. Hu and X. Jiang, A review of wind turbine icing and anti/de-icing technologies, *Energies*, 2024, **17**(12), 2805, DOI: 10.3390/en17122805.
8 R. Veerakumar, L. Tian, H. Hu, Y. Liu and H. Hu, An experimental study of dynamic icing process on an Aluminum-Conductor-Steel-Reinforced power cable with twisted outer strands, *Exp. Therm. Fluid Sci.*, 2023, **142**, 110823, DOI: 10.1016/j.expthermflusci.2022.110823.
9 Y. Liu, W. Chen, Y. Peng and H. Hu, An experimental study on the dynamic ice accretion processes on bridge cables with different surface modifications, *J. Wind Eng. Ind. Aerodyn.*, 2019, **190**, 218–229, DOI: 10.1016/j.jweia.2019.05.007.
10 Y. Peng, R. Veerakumar, Y. Liu, X. He and H. Hu, An experimental study on dynamic ice accretion and its effects on the aerodynamic characteristics of stay cables with and without helical fillets, *J. Wind Eng. Ind. Aerodyn.*, 2020, **205**, 104326, DOI: 10.1016/j.jweia.2020.104326.
11 Z. Goraj, An overview of the deicing and anti-icing technologies with prospects for the future. 24th International Congress of The Aeronautical Sciences, 2004, 29. Available from: https://www.icas.org/icas_archive/ICAS2004/PAPERS/547.PDF.
12 L. Vertuccio, F. Foglia, R. Pantani and L. Guadagno, New aircraft anti/de-icing technologies, *IOP Conf. Ser.:Mater. Sci. Eng.*, 2021, **1024**(1), 012012Available from:.
13 Z. J. Wang, D. J. Kwon, K. L. DeVries and J. M. Park, Frost formation and anti-icing performance of a hydrophobic coating on aluminum, *Exp. Therm. Fluid Sci.*, 2015, **60**, 132–137, DOI: 10.1016/j.expthermflusci.2014.09.003.
14 K. Morita and H. Sakaue, Characterization method of hydrophobic anti-icing coatings, *Rev. Sci. Instrum.*, 2015, **86**(11), 115108, DOI: 10.1063/1.4935585.
15 V. Vyas, K. Chauhan and S. Rawal, Advances in hydrophobic thin film coatings: A review on anti-icing surface technologies, *Mater. Today: Proc.*, 2024, DOI: 10.1016/j.matpr.2024.05.078.
16 C. Wei, B. Jin, Q. Zhang, X. Zhan and F. Chen, Anti-icing performance of super-wetting surfaces from icing-resistance to ice-phobic aspects: Robust hydrophobic or slippery surfaces, *J. Alloys Compd.*, 2018, **765**, 721–730, DOI: 10.1016/j.jallcom.2018.06.041.
17 J. Huang, L. Wang and J. Hu, Numerical investigation of droplet impact dynamics on Janus-textured heated substrates, *Phys. Fluids*, 2023, **35**(10), 107134, DOI: 10.1063/5.0170171.
18 J. Wang, L. Wang, J. Huang and D. Li, Droplet impact behavior on a hydrophobic plate with a wettability-patterned orifice: A lattice Boltzmann study, *Int. Commun. Heat Mass Transfer*, 2024, **159**(C), 108249.
19 Y. Lin, H. Chen, G. Wang and A. Liu, Recent progress in preparation and anti-icing applications of superhydrophobic coatings, *Coatings*, 2018, **8**(6), 208, DOI: 10.3390/coatings8060208.
20 Y. Liu, Z. Zhang, H. Hu, H. Hu, A. Samanta, Q. Wang and H. Ding, An experimental study to characterize a surface treated with a novel laser surface texturing technique: Water repellency and reduced ice adhesion, *Surf. Coat. Technol.*, 2019, **374**, 634–644, DOI: 10.1016/j.surfcoat.2019.06.046.
21 F. Piscitelli, A. Chiariello, D. Dabkowski, G. Corraro, F. Marra and L. Di Palma, Superhydrophobic coatings as anti-icing systems for small aircraft, *Aerospace*, 2020, **7**(1), 2, DOI: 10.3390/aerospace7010002.
22 Y. Liu and H. Hu, in Experimental investigations on bio-inspired icephobic coatings for aircraft inflight icing mitigation, ed. Mittal K. L. and Choi C. H., *Ice Adhesion: Mechanism, Measurement and Mitigation*, John Wiley & Sons, Ltd, 2020, pp. 547–575, DOI: 10.1002/9781119640523.ch18.
23 S. Moghtadernejad, C. Lee and M. Jadidi, An introduction of droplet impact dynamics to engineering students, *Fluids*, 2020, **5**(3), 107, DOI: 10.3390/fluids5030107.
24 H. Zhao, X. Han, J. Li, W. Li, T. Huang and P. Yu, *et al.*, Numerical investigation of a droplet impacting obliquely on a horizontal solid surface, *Phys. Rev. Fluids*, 2022, **7**(1), 013601, DOI: 10.1103/PhysRevFluids.7.013601.
25 B. J. Wei, Z. Liu, S. H. Shi, S. R. Gao, Y. F. Wang and Y. R. Yang, *et al.*, Droplet impact outcomes: Effect of wettability and Weber number, *Phys. Fluids*, 2024, **36**(7), 077144, DOI: 10.1063/5.0217564.
26 J. E. McDonald, Homogeneous nucleation of supercooled water drops, *J. Atmos. Sci.*, 1953, **10**(6), 416–433, DOI: 10.1175/1520-0469(1953)010<0416:HNOSWD>2.0.CO;2.
27 S. Jung, M. K. Tiwari, N. V. Doan and D. Poulikakos, Mechanism of supercooled droplet freezing on surfaces, *Nat. Commun.*, 2012, **3**(1), 615, DOI: 10.1038/ncomms1630.
28 L. Wang, F. Wang, C. Lu and H. Liu, Nucleation in supercooled water triggered by mechanical impact: Experimental and theoretical analyses, *J. Energy Storage*, 2022, **52**(A), 104755, DOI: 10.1016/j.est.2022.104755.
29 X. Zhang, X. Liu, X. Wu and J. Min, Impacting-freezing dynamics of a supercooled water droplet on a cold surface: Rebound and adhesion, *Int. J. Heat Mass Transfer*, 2020, **158**, 119997, DOI: 10.1016/j.ijheatmasstransfer.2020.119997.
30 N. B. Vargaftik, B. N. Volkov and L. D. Voljak, International tables of the surface tension of water, *J. Phys. Chem. Ref. Data*, 1983, **12**(3), 817–820, DOI: 10.1063/1.555688.
31 F. M. White, *Fluid mechanics*, 3rd edn, McGraw Hill Inc., New York, 1994.
32 M. W. Yang and S. Y. Lin, A method for correcting the contact angle from the $\theta/2$ method, *Colloids Surf., A*, 2003, **220**(1–3), 199–210, DOI: 10.1016/S0927-7757(03)00064-5.
33 I. Kåsa, A circle fitting procedure and its error analysis, *IEEE Trans. Instrum. Meas.*, 1976, **IM-25**(1), 8–14. Available from:.
34 D. Umbach and K. N. Jones, A few methods for fitting circles to data, *IEEE Trans. Instrum. Meas.*, 2003, **52**(6), 1881–1885.

Available from: https://ieeexplore.ieee.org/abstract/document/1246564.

35 J. D. Benther, J. D. Pelaez-Restrepo, C. Stanley and G. Rosengarten, Heat transfer during multiple droplet impingement and spray cooling: Review and prospects for enhanced surfaces, *Int. J. Heat Mass Transfer*, 2021, **178**, 121587, DOI: 10.1016/j.ijheatmasstransfer.2021.121587.

36 G. Charalampous and Y. Hardalupas, Collisions of droplets on spherical particles, *Phys. Fluids*, 2017, **29**(10), 103305, DOI: 10.1063/1.5005124.

37 H. Jones, Cooling, freezing and substrate impact of droplets formed by rotary atomization, *J. Phys. D: Appl. Phys.*, 1971, **4**(11), 1657, DOI: 10.1088/0022-3727/4/11/206.

38 D. Banks, C. Ajawara, R. Sanchez, H. Surti and G. Aguilar, Effects of liquid and surface characteristics on oscillation behavior of droplets upon impact, *Atomization Sprays*, 2014, **24**(10), 895–913, DOI: 10.1615/AtomizSpr.2014007590.

39 S. Lin, B. Zhao, S. Zou, J. Guo, Z. Wei and L. Chen, Impact of viscous droplets on different wettable surfaces: Impact phenomena, the maximum spreading factor, spreading time and post-impact oscillation, *J. Colloid Interface Sci.*, 2018, **516**, 86–97, DOI: 10.1016/j.jcis.2017.12.086.

40 Z. Yin, R. Su, W. Zhang, Z. Ding, F. Chai and Q. Chen, *et al.*, Oscillation characteristics of single droplet impacting vertically on smooth surfaces using volume of fluid method, *Microgravity Sci. Technol.*, 2021, **33**(5), 58, DOI: 10.1007/s12217-021-09901-8.

41 B. Gorin, D. Bonn and H. Kellay, Droplet impacts on cold surfaces, *J. Fluid Mech.*, 2022, **944**, A23, DOI: 10.1017/jfm.2022.493.

42 C. Wang, K. Li, H. Cai, Y. Wu, Z. Lin and S. Li, Study of supercooling phenomena in soil-water systems based on nucleation theory: Quantifying supercooling degree, *Water Resour. Res.*, 2023, **59**(11), e2023WR035935, DOI: 10.1029/2023WR035935.

43 Z. Zhu, X. Zhang, Y. Zhao, X. Huang and C. Yang, Freezing characteristics of deposited water droplets on hydrophilic and hydrophobic cold surfaces, *Int. J. Therm. Sci.*, 2022, **171**, 107241, DOI: 10.1016/j.ijthermalsci.2021.107241.

44 C. Sahay and S. Ghosh, Understanding surface quality: Beyond average roughness (Ra). 2018 ASEE Annual Conference & Exposition; 2018. Available from: https://peer.asee.org/understanding-surface-quality-beyond-average-roughness-ra.pdf.

45 M. Yuan, A. Dai, L. Liao, Y. Chen and X. Ji, Numerical study on surface roughness measurement based on nonlinear ultrasonics in through-transmission and pulse-echo modes, *Materials*, 2021, **14**(17), 4855, DOI: 10.3390/ma14174855.

46 Y. Liu, K. Zhang, W. Tian and H. Hu, An experimental investigation on the dynamic ice accretion and unsteady heat transfer over an airfoil surface with embedded initial ice roughness, *Int. J. Heat Mass Transfer*, 2020, **146**, 118900, DOI: 10.1016/j.ijheatmasstransfer.2019.118900.

